

Mineralogical and compositional changes in bones exposed on soil surfaces in Amboseli National Park, Kenya: diagenetic mechanisms and the role of sediment pore fluids

Clive N.G. Trueman^{a*}, Anna K. Behrensmeyer^b, Noreen Tuross^c, Steve Weiner^d

^a School of Earth and Environmental Sciences, University of Portsmouth, Burnaby Building, Portsmouth PO1 3QL, UK

^b Department of Paleobiology, National Museum of Natural History, Smithsonian Institution, P.O. Box 37012, Washington, DC 20013-7012, USA

^c Laboratories of Analytical Biology, National Museum of Natural History, Smithsonian Institution, Washington, DC 20560, USA

^d Department of Structural Biology, Weizmann Institute of Science, Rehovot 76100, Israel

Received 23 March 2003; received in revised form 6 November 2003; accepted 12 November 2003

Abstract

Bones exposed on tropical savannah grasslands of Amboseli National Park, Kenya undergo extensive post-mortem alteration within 40 years. A combined analytical approach involving TEM microscopy, trace metal analysis, FTIR spectroscopy, and petrographic analysis has revealed a complex, dynamic diagenetic environment operating within exposed bones, driven by evaporative transport of soil water from the bone/soil interface to the upper exposed surface of the bone. This process results in extensive bone/soil-water interaction, and is responsible for increases in the concentrations of trace elements such as Ba and La of 100 – >1000% within 15 years. The maximum and mean size of bone crystallites increases with continued exposure. This change in mean crystallite length is correlated positively with increases in bone crystallinity, which in turn is associated with degradation of the bone protein. Microbial decomposition is rarely observed in the Amboseli bones, but where present resulted in severe dissolution–reprecipitation of bone mineral. Many bones showed extensive permineralization of the larger vascular spaces with calcite and barite and, to a lesser extent, crandallite. Permineralization of unburied bones may account for 95% reduction in macro (micron–millimeter scale) porosity in the bone within 2 years of death.

We produce a model for pre-burial diagenesis of bone in arid tropical environments that highlights extensive alteration of bone chemistry within 1–40 years post-mortem.

© 2003 Elsevier Ltd. All rights reserved.

Keywords: Bone; Diagenesis; Crystallinity; Collagen; Trace elements; Permineralization; Amboseli

1. Introduction

The chemical composition of bone is used to reconstruct diverse aspects of the biology, ecology, taphonomy and environment of vertebrate remains (e.g. [7,33,46]). Many studies of ancient bone and tooth chemistry focus on pre-mortem biogenic signals as records of paleodiet [33,39,37], migration [15,19,23] paleophysiology [1], paleoclimate [9,26], or to support ancient biomolecule analysis [12,38] and radiocarbon

dating. Other studies exploit the post-mortem diagenetic chemistry of bone to reconstruct the paleoenvironment of burial [54], calibrate potential error in U-series dating [27], or establish provenance of disputed bones [32,44]. Successful application of these techniques requires a thorough understanding of the processes affecting bone after death, the mechanisms by which bone alteration occurs and the rates of alteration.

Bone is unstable once removed from the body, and the main changes that occur during the diagenesis of bone are well known, consisting of loss of organic material, increase in crystallinity of bone mineral, changes in bone porosity, and changes in trace element composition (e.g. [17,25,47,48]). The diagenesis

* Corresponding author. Tel.: +44-2392-842-293; fax: +44-2394-842-244.

E-mail address: clive.trueman@port.ac.uk (C.N.G. Trueman).

of buried bone (as opposed to bone exposed on the soil surface) has been studied extensively, and recent advances in this field include the recognition of the role of the hydrological environment of burial [17,29], the intimate association between alteration of the mineral and organic components of bone [13], and the role of micro-organisms in diagenesis [11,17]. Less is known, however, regarding processes that may change bone structure and chemical composition prior to burial.

The effects of surface weathering have been monitored extensively in a series of bones exposed on tropical savanna soils at Amboseli National Park, Kenya, for up to 40 years ([2,4]; unpublished data). The effects of weathering on the mineralogy, organic content, trace element content, and stable isotope compositions of these bones have also been investigated [24,47,48]. These previous studies indicated that the Amboseli bones have undergone measurable changes in crystallinity, organic content and trace element compositions over the collection period. This assemblage of bones has a number of distinct advantages as a test case for the study of diagenesis. Most of the marked bones were completely destroyed by physical weathering processes by the end of the observation period, so that samples collected in successive years during the experiments likely represent the full range of alteration that will be encountered during natural surface exposure. The absolute duration of exposure is known for each collected bone, the rainfall was monitored throughout the collection period, and periodic measurements of pH and soil temperature were performed. We have used the bones from the natural weathering experiments at Amboseli to investigate further the nature and mechanisms of post-mortem alteration of bones on the soil surface. We then use this information to infer the major processes responsible for pre-burial alteration of bone and propose a model for the chemical alteration of skeletal remains exposed for periods of decades on soil surfaces. In this study, we investigate post-mortem alteration in bone *sensu stricto* (as distinct from enamel and/or dentine).

1.1. The environment at Amboseli

Amboseli National Park lies in a depression north of Mt. Kilimanjaro along the border of Kenya and Tanzania, and includes habitats ranging from swamp to woodlands to open grasslands and thornbush [3–6]. The climate is semiarid, with average monthly temperatures ranging from 26 to 34°C and average rainfall of 350–400 mm/y [53]. Soil waters are mainly alkaline, and range from pH 6.5 in swamps to pH >9 in soils adjacent to Lake Amboseli [42]. During the dry season, salt crusts form at the surface where there are high rates of evaporation through the soil, e.g., in areas bordering the swamps.

2. Materials and methods

Bones from nine carcasses of large mammals were examined in this study, and details of the skeletons examined are provided in Table 1. Following collection over the period between 1975 and 2001, bones were stored in the Kenya National Museum in Nairobi or at the National Museum of Natural History in Washington, DC. A portion of bone was removed from these specimens, one half was embedded in epoxy-resin, and thin sections and polished thick sections were prepared. The remaining portion of bone was retained for chemical and mineralogical analyses, which were performed on the first and last bones collected within a weathering sequence. Where possible, three separate samples were taken from each bone. A sample of bone from the weathered (upper, exposed) surface was removed by scraping the surface with a razor or saw blade to a depth of no more than 1 mm. A second sample was taken from the sub-surface cortical portions of bone, and a final sample was taken of trabecular bone. Where possible ~0.5 g of bone chips or bone powder were used in analyses described below.

Bone samples were ground, split into two, and one half was treated overnight with 3–5 ml of sodium acetate buffer adjusted to pH 5 with acetic acid. After treatment, the sample was centrifuged at 12,000 rpm, and the supernatant removed; the remaining solid was washed three times with distilled water and dried. Bone samples were characterized by fourier transform infra red spectroscopy (FTIR), Thermogravimetric analysis (TGA) and differential thermal analysis (DTA). Bone crystal size was determined by direct measurement of disaggregated crystals imaged by transmission electron microscopy (TEM). Trace element compositions were determined by inductively coupled plasma mass spectrometry (ICP-MS). In addition bone samples were examined in thin section. Details of analytical procedures are given in Appendix A.

3. Results

3.1. Microbial alteration

Sixty-six thin sections from 10 skeletons were examined with transmitted light microscopy for traces of microbial alteration. Only skeletons C75-7 and C75-11 showed any such traces, and in skeleton C75-7, microbial alteration was found only in the bone recovered in 1982. Bones from skeleton C75-11, however, show extensive alteration in all years of collection except 1980. Microbial alteration is manifested as circular or oval destructive foci c. 20 µm in diameter. These foci are surrounded by a relatively dense mineralized apatite wall or ‘cuff’ [18]. Foci are the cross sections of tunnels mostly oriented longitudinally, parallel to the osteonal

Table 1

Summary of specimens investigated in this study and their diagenetic state. In addition to samples described below, petrographic thin sections were made from bones recovered in years between first and last sampling.

Sample	Species	Year collected	Bone portion	Bioerosion? (Y/N)	Authigenic minerals (C, CD, D, T, B)	Crystallinity IRSF	Wt% organic content (FTIR)	Wt% organic content (TGA)	Crystal size						
									mean l,w (nm)	range l (nm)	(n)				
C75-2	Cow, <i>Bos</i> sp.	1975	1	N	C, D, T	2.7	27	20	40, 22	11-92	91				
			2	N		2.8	34								
			3	N											
		1990	1	N					2.9	20					
			2	N		3	24								
			3	N		3.1	20		45, 24	11-98	106				
		2001	1	N											
		2	N												
		3	N												
C75-3	Elephant, <i>Loxodonta africana</i>	1975	1	N	C, B	2.8	28	20	43, 22	14-96	89				
			2	N		2.9	33								
			3	N		2.8	27								
		1990	1	N		3.1	16		20						
			2	N											
			3	N											
		2001	1	N		3	17								
			2	N		3	17								
			3	N											
C75-6	Elephant, <i>Loxodonta africana</i>	1975	1	N	C, B			2.8	29	30	52, 24	17-114	115		
			2	N		2.7	28								
			3	N		2.75	31								
		1990	1	N		3.2	15.5	15							
			1B	N											
			2	N					2.9		19				
		3	N	3		24									
		C75-10	Zebra, <i>Equus burchellii</i>	1975		1	N	C, D, B	2.7		31	18	38, 23	19-106	127
						2	N								
3	N														
1990	1			N	3.3	17									
	1b			N	2.9	22									
	2			N	3.1	22									
3	N			3.1	22.5										
1975	1					Y	C, D, B		2.9	15	18		31, 18	13-63	73
	2					Y			2.9	24					
	3	Y	2.9	23											
1996	1	Y	3.3	17	17										
	2	Y				3.1	23								
	3	Y				3.1	22.5								

Table 1 (continued)

Sample	Species	Year collected	Bone portion	Bioerosion? (Y/N)	Authigenic minerals (C, CD, D, T, B)	Crystallinity IRSF	Wt% organic content (FTIR)	Wt% organic content (TGA)	Crystal size				
									mean l,w (nm)	range l (nm)	(n)		
C75-12	Wildebeeste, <i>Connochaetes taurinus</i>	1975	1	N	C, D, B, Cd, T	2.9	21		43, 22	19–99	129		
			2	N		2.9	30						
			3	N									
		1990	1	N		3.4	15		53, 26	8–128	127		
			2	N		2.8	25						
			3	N		2.9	24						
C75-14	Buffalo, <i>Syncerus caffer</i>	1975	1	N	3.1	21	24						
			1b	N	3	23	24						
			2	N	2.9	27							
		1990	3	N	2.9	28	18						
			1	N	3.2	17							
			2	N	2.9	20							
C75-27	Elephant, <i>Loxodonta africana</i>	1977	1	N	2.8	23	26	42, 23	14–105	46			
			2	N	2.8	28							
			3	N									
		1990	1	N	2.8	23	20		40, 21	17–81	102		
			2	N	3	25							
			3	N									
C76-1	Rhinoceros, <i>Diceros bicornis</i>	1975	1	N			20	19					
			2	N									
			3	N									
		1990	1	N		2.9	23	22	14				
			1b	N		3.1	14						
			2	N		2.9	28						
		2001	3	N		2.8	33	21					
			1	N		2.9	17						
			2	N									
		2001B	3	N		2.9	18	16					
			1	N		3	15						
			2	N		3	18						
			3	N	2.9	21							

Sample code: 1=sample scraped from outer surface of bone; 2=sample of cortical bone >5mm from outer surface; 3=sample of trabecular bone. Authigenic minerals; C=calcite, CD=crandallite, D=dahlite, T=trona, B=barite. Crystal size: l=length, w=width.

canals. The tunnel interiors are frequently filled with secondary apatite, which may appear more electron-dense than surrounding bone apatite in back scattered electron (BSE) imaging. The microbial alteration features seen in C75-11 are essentially identical to features recognized in several studies of archaeological and fossil bone [8,17,18,30,45,49].

3.2. Authigenic minerals

The minerals calcite (CaCO_3), barite (BaSO_4), dahllite ($\text{Ca}_{10}(\text{PO}_4\text{CO}_3)_6(\text{OH})_2$), crandallite ($\text{Ca}_2\text{Al}_2(\text{PO}_4)_2(\text{CO}_3)_2(\text{OH},\text{F})_2$), trona ($\text{Na}_3\text{CO}_3\text{HCO}_3\cdot 2\text{H}_2\text{O}$) and possibly sepiolite ($\text{Mg}_4\text{Si}_6\text{O}_{13}(\text{OH})\cdot 6\text{H}_2\text{O}$) have all been identified by thin section petrography, FTIR spectroscopy, and EDS analysis in void spaces (e.g., osteonal canals, trabecular spaces) in bones from Amboseli.

3.2.1. Calcite

Calcite is the most common authigenic mineral in bones from Amboseli, found in approximately half of all thin sections. The extent of calcite present in each section varies from minor calcite developed as a thin crust on detrital particles within trabecular spaces, to extensive sparry calcite completely filling most osteonal cavities. Calcite is found as a microcrystalline material at bone surfaces (internal and external), progressively advancing into the interior of the bone, exploiting cracks that develop around osteonal margins and along structural weaknesses in the bone. Calcite is also commonly developed as a void filling material in osteonal cavities. In this case calcite mineralization apparently nucleates on the bony wall of the osteonal canal, and calcite crystals grow into the center of the canal.

3.2.2. Barite

Barite is the second most abundant authigenic mineral, identified in more than a third of all thin sections. Barite is always found within void spaces, especially osteonal spaces, and is developed as euhedral crystals constrained by the boundaries of the cavities. Barite is concentrated in the osteonal cavities located close to, but not immediately at, the external surfaces of bones. Barite and calcite are often found associated in the same bone, although rarely intergrown. Both barite and calcite can develop rapidly in the bones. A rib fragment recovered from C75-6 (1975), shows extensive development of barite and calcite within osteonal cavities only 1–2 years post mortem.

3.2.3. Dahllite and crandallite

The minerals dahllite and crandallite are sparingly developed as authigenic minerals in bones from Amboseli, although these minerals can be difficult to distinguish petrographically from original bone mineral (also dahllite), and authigenic barite. Authigenic dahllite

is developed as a secondary infilling mineral in biogenic destructive tunnels in bone from skeleton C75-11, and in authigenic mineral crusts formed on external exposed surfaces of bones C75-2 (2001) and C75-12 (1990).

Crandallite is found in bones from only one skeleton, C75-12, where it is present in trabecular voids close to the exposed surface of the bone (sampled in 1990), and possibly within a mineral crust adhering to the bone sampled in 1985. The mineral crust developed around the vertebra C75-12 (1985) consists mainly of a Ca-rich clay (probably montmorillonite), trona, detrital feldspars, potassium salts, and calcite. There is no evidence of widespread redistribution of phosphate from the bone into the weathering crust.

3.2.4. Trona

Trona is a water-soluble sodium carbonate evaporite mineral. Trona is extensively developed at and near the upper (exposed) surface of bone C75-12 (1990), and is associated with authigenic apatite at the exposed surfaces of bones C75-12 (1990) and C75-2 (2001). Trona is developed as translucent euhedral crystals growing into void spaces, and is evident in hand specimens as a powdery-white crust that is easily abraded. Trona has high birefringence colors and can be mistaken for calcite in thin section.

3.2.5. Sepiolite

Sepiolite is a magnesium silicate mineral with clay-like properties. The Amboseli region is famous for the large deposits of sepiolite and palygorskite (Meerschaum) that are commercially exploited [16,42]. Sepiolite has been identified within bones from Amboseli by EDS-SEM, but it is unclear whether this sepiolite is detrital or authigenic.

3.3. Bone mineral

All of the bones sampled from Amboseli are composed principally of carbonated hydroxyl-apatite (dahllite). Calcite was positively identified in some samples through the presence of the characteristic (weak) absorbance at 713 cm^{-1} . In other samples, however, the presence of authigenic calcite was inferred from anomalously high values of the carbonate absorbance at $\sim 1415\text{ cm}^{-1}$. The crystallinity of bone mineral, determined by the infra red splitting factor (IRSF, [52]), ranged from 2.7 to 3.4 (Table 1). All bones collected within two years of death have values for the IRSF of 2.8 or less (typical of fresh osteonal bone e.g. [41,56]). There is no significant difference in IRSF between the three portions of bone sampled (surface and sub-surface samples of cortical bone, and trabecular bone) in these relatively fresh samples. The IRSF of bone dahllite increases with increasing exposure and weathering. Samples from the last year of collection show significantly higher values (Student's *t*-test $P \ll 0.001$) for the

IRSF, and most of this increase is seen in samples from the bone surface (Table 1). Stiner et al. [41] also noted that surface regions of bones weathered for 2 and 9 years showed higher values for the IRSF than internal portions of the same bone. Bones that were initially recovered several years post-mortem yield anomalously high IRSF values when compared to bones recovered within 2 years of death, and again this difference is most clearly expressed in samples from the outermost bone surface.

The carbonate content of bone mineral could not be estimated reliably from FTIR spectra using the method of Wright and Schwartz [55]. The intensity of peaks corresponding to the ν_3 and ν_2 carbonate absorbances (1415 and 875 cm^{-1} respectively) is only weakly correlated, suggesting some interference on one of the two peaks. This is most likely from the organic matrix absorbance (probably C-H vibrations) superimposed on the $\nu_3\text{CO}_3$ absorbance at 1415 cm^{-1} . Consequently total carbonate contents estimated from the FTIR measurements are overestimates and appear to co-vary with organic matrix contents.

3.4. Organic content of bone

The amount of organic material remaining in the surface bone samples ranged from $\sim 27\%$ wt in fresh samples to 13% wt in samples from the last year of collection (Table 1). Samples collected 5 or more years after death have a relatively low organic content. The ratio of the intensities of the $\nu_1\text{Amide}$ (1640 cm^{-1}) and $\nu_3\text{PO}_4$ (1035 cm^{-1}) absorbance peaks (Am/P) in the FTIR spectra of bone are positively correlated with the organic/mineral weight ratio determined by TGA ($r^2=0.86$). A least-squares line fitted through the data (Fig. 1B) yields the relationship:

$$\text{Weight \% organic} = 11.06 \ln(\text{Am/P}) + 32.43$$

This relationship is valid at least for bones with >15 wt% organic material, however, at low organic contents the logarithmic curve is constrained by just one value obtained from a fossil (c. 100 Myr old) bone.

The ratio of the intensities of the $\nu_1\text{Amide}$ and $\nu_3\text{PO}_4$ absorbances in bone samples range from 0.8 to 0.2, equivalent to ~ 30 and ~ 15 wt% organic material, respectively (Table 1). Bone surface samples show the greatest change in organic material contents (about 50% reduction over the collection period), however, sub-surface cortical bone samples also show $\sim 25\%$ loss of organic material (from 30 wt% to 23 wt%) through the collection period.

3.5. Bone crystal sizes

Bone crystals are plate-shaped in all samples, regardless of species or duration of exposure (Fig. 2). Crystal

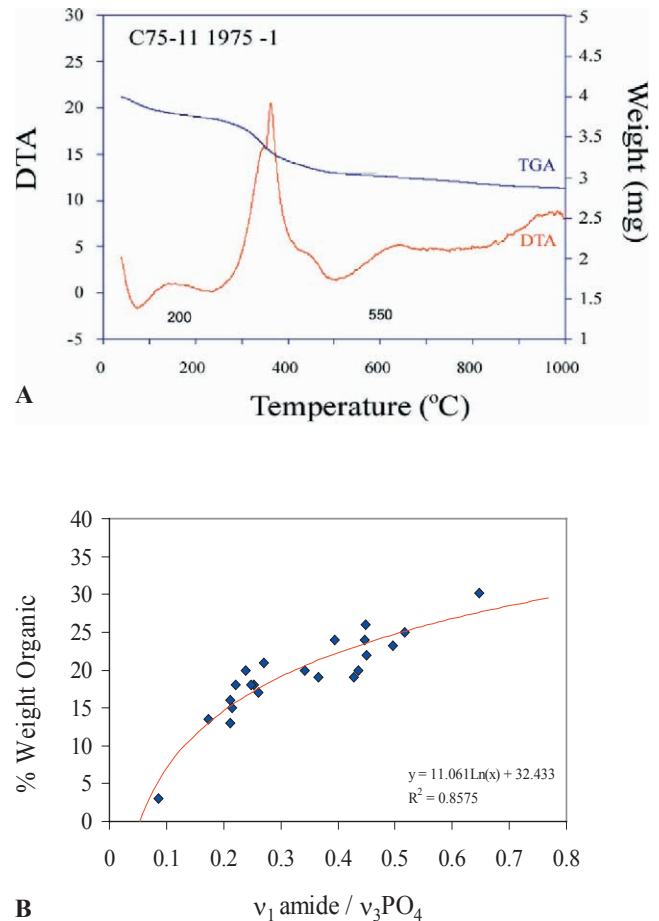


Fig. 1. (A) TGA (upper curve) and DTA (lower curve) analyses of bone C75-11 (1975)-1. TGA (right hand axis) monitors weight change with heating, and DTA shows the energy adsorbed or released by the sample during heating. Note that the main release of energy (associated with combustion of the organic matrix) occurs between 200 and 550 °C. The weight change occurring between these temperatures was therefore used as an estimate of the amount of organic material present in the sample. (B) Relationship between % weight loss between 200 and 550 °C (determined by TGA) and the ratio of the intensities of the $\nu_1\text{Amide}/\nu_3\text{PO}_4$ absorbance peaks determined by FTIR spectroscopy.

lengths range from <10 – ~ 100 nm, with average lengths ~ 40 nm and average widths ~ 30 nm. A small proportion of crystals on all TEM grids appear needle-shaped, approximately 30 nm long and <10 nm wide. These crystals are all relatively electron dense, however, and are clearly plate-shaped crystals oriented with the thin edges of the crystals roughly parallel to the electron beam (e.g. [51,56], Fig. 2C and D).

Crystal dimensions (length and width) were measured in bone surface samples taken from the first and last years of collection for 5 skeletons (C75-2, 6, 11, 12, and 27, Fig. 3). Simple ANOVA indicates that the crystal lengths are significantly different between individual bones ($P<0.001$). The average and maximum crystal length increased over time in skeletons C75-2, 6, 11, and 12 (significant difference in means between first and last year of collection at $P<0.01$; Student's t -test);

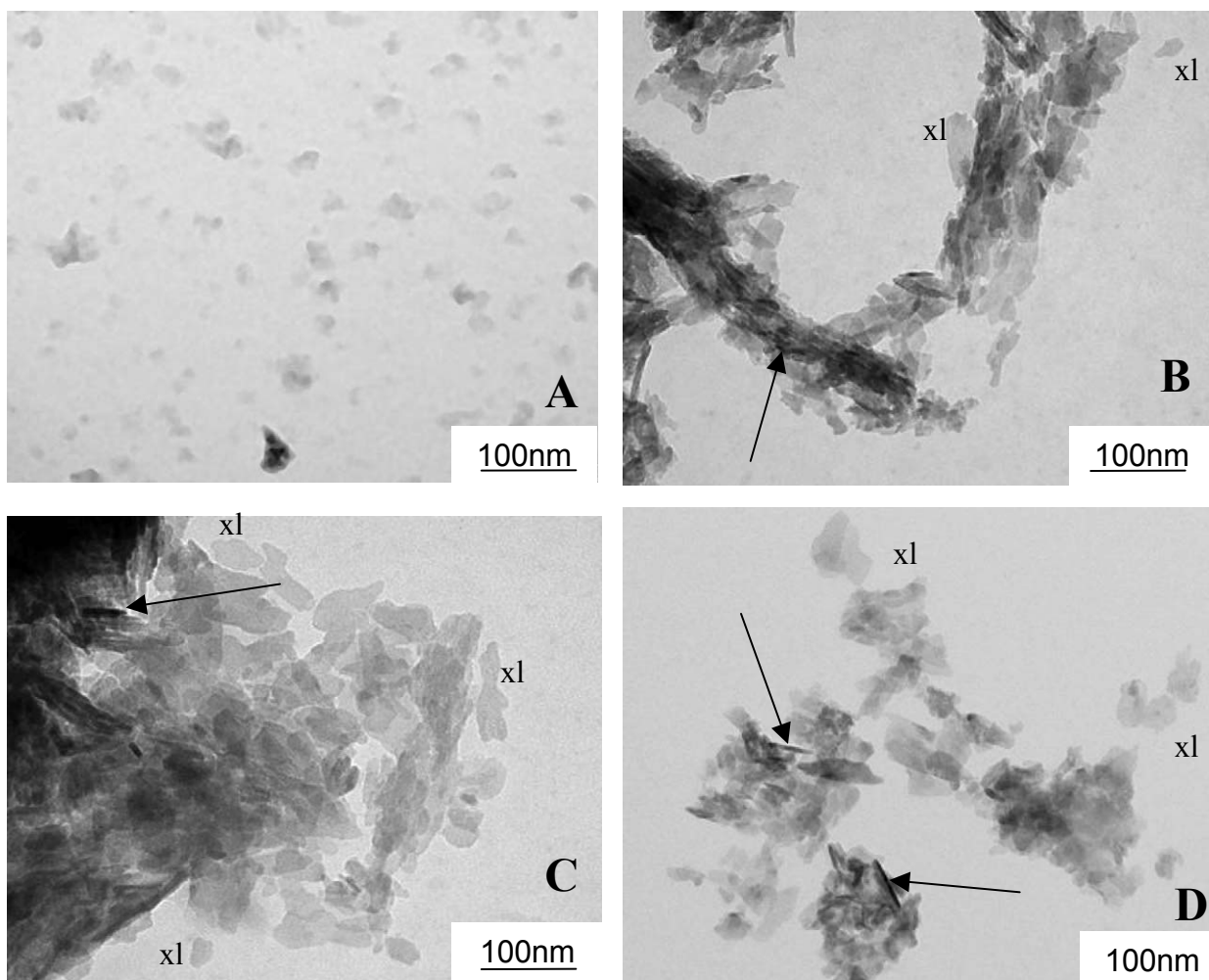


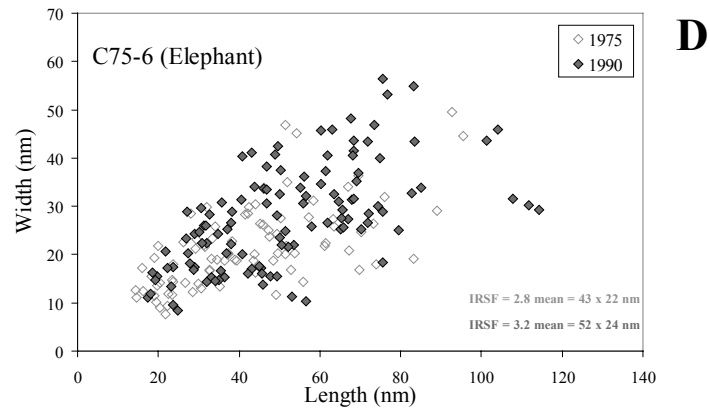
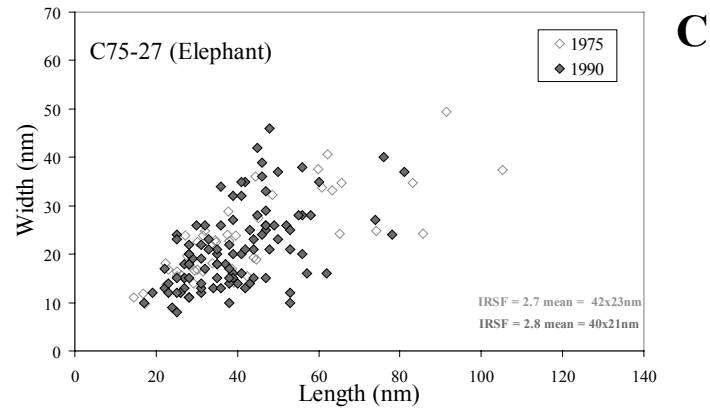
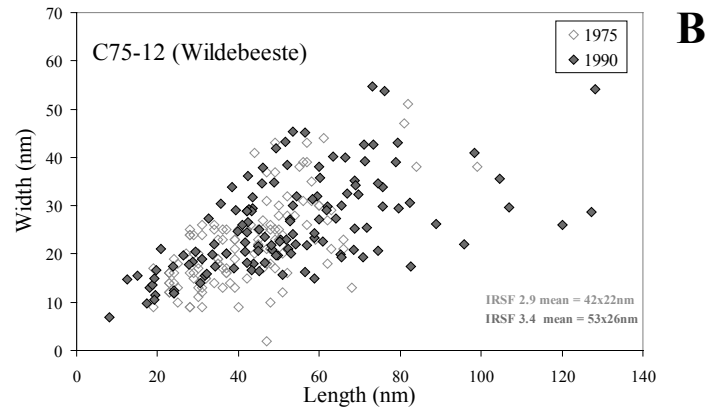
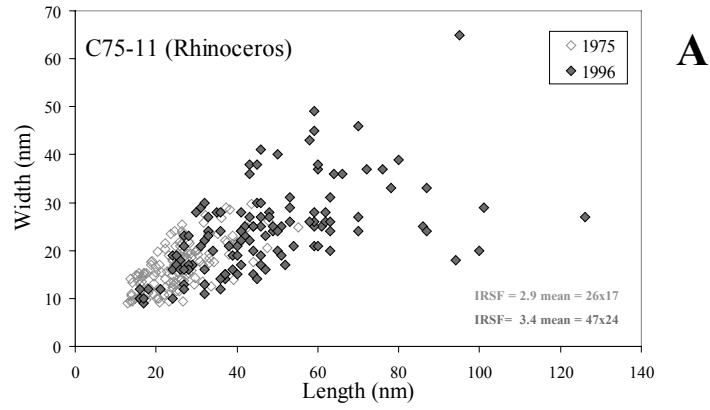
Fig. 2. TEM images of bone crystals isolated from bones C75-11 (1975) (A) C75-12 (1975) (B), C75-11 (1996) (C), and C75-6 (1990) (D). Sample (A) was completely disaggregated during the preparation procedure and almost all crystals are isolated, single crystals. In most other cases bone crystals remained as aggregated clusters of crystals sometimes associated with collagen fibrils (e.g. B arrow), despite long sonication times. Examples of crystals available for measurement are indicated (xl). In all cases crystals are plate shaped, usually lying on the large crystal face. Crystals lying with their thin faces parallel to the electron beam appear as electron dense needles (C and D arrowed).

but showed no significant change in skeleton C75-27 (Table 1, Fig. 3C). The largest crystals in samples C75-11 and 12 were found in bones from the final year of collection, and these crystals are relatively narrow (length/width ratio of 3–5) compared to crystals from fresh bone (length/width ratio of 1.7–2) (Fig. 3A, B). No significant change in length/width ratio was seen in crystals from C75-2 or C75-6. The mean crystal length in general increased from around 40nm to around 50nm within the duration of exposure, and there is a clear positive relationship between IRSF and mean crystal length (Fig. 4, excluding the single outlier C75-11 (1975), $r^2=0.9$).

Bones with lower organic contents could respond to the preparation methods differently, in particular by releasing a greater proportion of larger crystals during sonication, and thus the observed increase in crystal size over time seen in our samples could potentially be an

artifact of the preparation. In this case, however, one would expect that the relationship between mean crystal length and protein content would be stronger than that between mean crystal length and IRSF. In fact, the opposite is true (correlation coefficients of 0.7 and 0.9 respectively). We conclude that the observed increases in mean crystal length reflect real changes in crystal dimensions within the bones.

The observed increase in mean crystal length may be due to either growth of crystals, or to the loss of smaller crystals (or both). Loss of the smallest crystals during weathering would produce an increased positive skew in the distribution of crystal lengths in the last year of collection compared to the initial year of collection. There is no clear relationship between changes in size distribution and mean crystal length during weathering, and consequently we believe that the increase in mean crystal size is not primarily caused by the loss of the



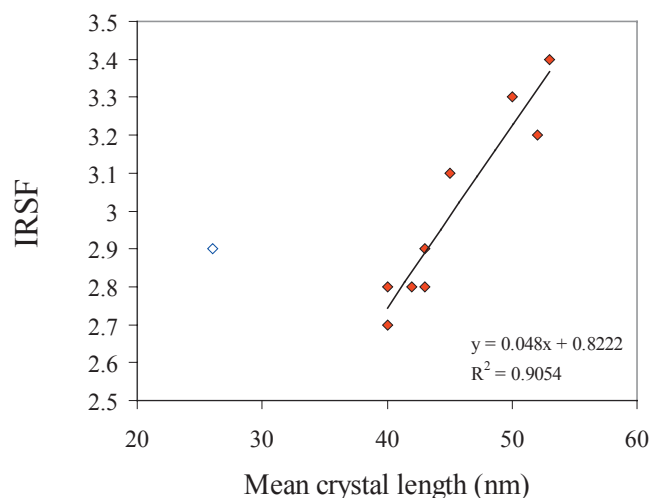


Fig. 4. Relationship between mean crystal length (nm) and IRSF. The single outlier is bone C75-11 (1975). This outlier may be an artifact of the bone's response to preparation (compare Fig. 3A–D), and/or may reflect taxonomic differences in the structure of the ribs of the black rhinoceros compared to other large African mammals.

smallest crystals within the population. The close relationship between IRSF and mean crystal length therefore indicates that IRSF is a measure of crystal growth.

3.6. Trace element composition

The initial concentration of Ba in bones of large mammals from Amboseli is typically 50–100 ppm, whereas concentrations in soils from Amboseli are around 500–1000 ppm (Table 2). Ba concentrations in bone do not show a clear pattern of change with increased exposure.

The concentrations of the REE in samples of surface, sub-surface cortical, and trabecular bone vary between sample types, and with age of exposure (Fig. 5, Table 2). The total REE concentration in the initial year of sampling is 1–5 ppm. The concentrations of the REE in the bones from skeletons C75-2, C75-6, C75-10, and C75-14 show clear increases in REE concentrations with exposure, and the largest increases are seen in trabecular bone, while the smallest increases are generally seen in the surface or sub-surface cortical samples (Fig. 6A). Interpretation of this increase is complicated, however, as the concentrations of the REE in the surrounding sediment are between one and two orders of magnitude greater than those in fresh bone. Thus contamination of the bone sample with sediment could increase the

apparent concentration of REE in bone. While care was taken to remove any attached sediment both mechanically and by treatment with buffered acid solutions, it is possible that some of the increase in REE concentrations is due to sediment contamination, especially in samples of porous trabecular bone. REE concentrations were higher in bone that had been buried than bone from the same skeleton (C76-1) that remained exposed for the duration of the weathering experiment.

If the trace element concentrations measured in bone samples were contaminated by sediment, one would expect that increases in the concentration of Ba would also be higher in the sub-surface and trabecular samples, and that the concentration of REE in bone would increase in proportion to their relative distribution in the sediment. In fact increases in the concentrations of Ba do not mirror increases in REE concentration (Fig. 6), and increases in REE concentrations in bone do not mirror their distribution in the sediment (Fig. 7). This suggests that the differences in REE concentration seen during exposure are not caused by contamination of samples by adhering sediment.

4. Discussion

Bones lying on the soil surface for 26 years or less undergo substantial physical and chemical changes, especially on their exposed surfaces. In the tropical grassland environment of Amboseli Park, most physico-chemical change appears to be abiotically rather than microbially mediated. The suite of authigenic minerals formed within the taphonomic bone series indicates that soil pore water is involved in the processes of bone alteration. The trace element composition of bone mineral is altered by the same pore-water interaction. It is important to note, however, that while extensive mineralogical and chemical alteration was seen in most bones after 15 years exposure, the principle agents responsible for *destruction* of bones on the soil surface at Amboseli are those associated with physical weathering. In this ecosystem, most bones are destroyed within 10–30 years post-mortem primarily because of physical rather than chemical or microbiological processes, although chemically mediated loss of collagen contributes to overall weakening of bone structure.

4.1. Mechanisms of bone mineral alteration

In many of the bones analyzed there is a major reduction in the organic matrix content during exposure

Fig. 3. Sizes (length and width) of crystals disaggregated from bone surfaces. Samples taken from the initial (open symbols) and final (filled symbols) years of collection. Note increase in mean size in bones taken from skeletons C75-12, C75-11, and C75-6, but no increase in mean size in bones from skeleton C75-27. Note also that the longest crystals in bones from skeleton C75-11 and C75-12 have higher length/width ratios compared to the main crystal population. Mean crystal length and widths are noted on graphs, together with crystallinity (IRSF) values.

Table 2
Trace element content (ppb) of bone and sediment samples from Amboseli

		Ba	La	Ce	Pr	Nd	Sm	Eu	Gd	Tb	Dy	Ho	Er	Tm	Yb	Lu	Total REE
C75-6	1975-1	48611.3	719.3	1245.5	135.4	505.1	97.9	23.2	83.1	13.3	77.6	16.3	39.8	5.8	30.3	4.9	3.0
	1975-3	44648.1	842.9	1320.8	136.8	544.4	104.5	25.5	95.5	15.6	93.5	19.9	54.3	7.8	46.5	7.6	3.3
	1990-1	67866.7	3055.6	5944.9	639.6	2317.6	423.7	108.4	299.4	44.3	268.3	53.0	128.5	17.6	102.1	14.5	13.4
C75-2	1990-3	52691.2	1896.8	3529.0	378.0	1353.0	259.6	66.0	194.6	29.9	180.1	37.2	93.9	12.3	73.9	11.4	8.1
	1976-1	114378.2	364.8	697.7	84.2	323.3	68.8	20.1	56.9	9.4	52.2	9.9	23.7	3.2	18.5	3.4	1.7
	1976-3	207542.5	200.0	412.0	51.7	218.8	58.1	21.4	68.7	10.5	59.2	11.7	28.7	3.7	20.8	4.3	1.2
C75-3	1996-1	121308.6	2200.0	3477.7	470.4	1663.4	302.4	81.4	220.9	31.9	183.5	34.6	81.4	10.5	66.5	9.7	8.8
	1996-3	127208.1	2573.9	4059.1	555.2	1998.3	361.4	92.7	258.7	38.8	221.2	40.5	95.8	13.7	75.7	11.8	10.4
	2001-1	315993.5	1639.2	3367.7	376.3	1355.1	260.2	69.1	195.7	29.0	174.7	35.2	88.7	12.4	77.2	12.4	7.7
C75-3	2001-2	129529.1	337.4	961.0	78.5	277.4	55.9	14.2	43.8	7.2	42.6	8.6	25.1	4.1	29.5	5.1	1.9
	2001-3	232034.1	9629.1	15058.7	2122.9	7693.3	1489.2	430.0	1203.1	178.9	1042.2	198.7	483.4	61.4	332.7	44.8	40.0
	1976-1	75257.1	1073.0	2457.5	240.6	908.3	168.2	44.4	129.1	18.7	118.6	22.7	56.6	8.0	47.9	7.6	5.3
C75-12	1976-3	76611.2	1311.8	3009.6	256.1	978.3	196.7	53.1	174.1	25.6	155.3	32.7	80.0	11.4	65.4	10.1	6.4
	1990-1	78821.9	1581.5	3304.3	329.4	1195.4	215.8	59.9	152.2	22.8	135.1	26.3	62.6	8.8	53.2	8.2	7.2
	1990-3	184531.0	14454.0	27468.8	2982.1	10595.1	1889.9	511.0	1373.2	197.1	1184.2	230.8	566.5	79.3	465.2	66.0	62.1
C75-12	2001-1	66459.4	1100.8	2210.0	233.3	829.0	146.7	40.0	101.0	15.8	86.4	16.9	40.9	6.1	34.3	5.5	4.9
	2001-2	96084.2	1815.9	3644.0	378.8	1365.7	239.3	66.7	174.0	25.1	148.0	28.2	68.1	9.3	57.0	9.0	8.0
	2001-3	115953.3	2963.0	5939.5	616.6	2234.3	394.0	109.1	305.2	44.1	258.8	51.6	127.6	18.2	102.4	15.8	13.2
C75-12	1976-1	198230.3	2120.2	4522.7	503.3	1848.6	357.6	89.4	278.9	41.2	241.5	47.6	123.8	18.0	100.6	16.4	10.3
	1976-1(2)	197476.4	1707.8	3955.8	401.8	1472.1	293.6	79.6	233.6	34.6	211.0	42.3	115.3	16.7	102.3	15.6	8.7
	1976-3	167474.3	2548.5	4821.3	569.8	2054.5	382.9	104.9	299.9	44.9	268.2	53.8	134.9	19.3	115.6	16.9	11.4
C76-1	1990-1	255784.8	1398.4	5399.2	328.3	1195.8	243.3	61.4	147.0	26.5	194.0	47.2	143.3	26.8	192.9	32.0	9.4
	1990-1(2)	345003.4	3692.2	8309.0	875.5	3159.3	589.1	149.4	388.8	59.9	381.1	74.5	194.1	29.5	193.5	30.7	18.1
	1990-3	188524.8	2562.7	5690.1	572.8	2098.4	395.5	106.1	274.2	46.3	268.4	56.6	137.5	23.7	136.9	23.0	12.4
C76-1	1976-1	49375.2	2417.9	5080.9	519.1	1853.9	335.4	85.9	228.8	33.9	188.7	37.3	90.0	13.2	81.8	11.6	11.0
	1976-3	25827.3	196.3	358.3	40.7	146.3	28.8	6.0	23.2	2.5	18.9	3.0	6.0	0.3	4.5	0.6	0.8
	1990-1	77373.3	2646.4	5129.5	546.4	1981.1	350.4	91.0	237.9	34.4	220.6	42.5	107.3	15.2	93.0	14.1	11.5
C76-1	1990-1(2)	52974.1	1610.8	3212.9	331.7	1194.8	212.7	55.6	147.8	22.7	135.0	26.4	67.4	10.2	61.6	10.3	7.1
	1990-3	99725.0	443.0	808.9	88.9	308.8	58.7	17.1	44.9	6.9	37.4	7.4	18.4	2.8	17.4	3.2	1.9
	2001-1	94222.0	3676.2	6797.5	746.2	2649.4	480.5	125.4	357.9	51.9	298.2	58.4	146.2	20.1	116.7	18.1	15.5
C76-1	2001-2	50467.6	1537.8	2925.3	322.7	1122.9	201.1	55.7	142.1	22.4	126.7	24.7	61.6	8.8	55.2	10.0	6.6
	2001bd-1	114026.0	4745.0	8893.9	965.5	3535.3	610.4	161.3	437.0	64.9	370.4	74.4	181.0	26.4	148.2	22.6	20.2
	2001bd-2	69121.2	5154.7	9571.9	1058.8	3788.0	673.9	173.9	480.0	68.4	387.1	75.0	179.7	25.4	150.5	22.2	21.8
C75-10	2001bd-3	150470.2	11961.3	22176.5	2459.9	8949.8	1574.4	414.3	1128.4	162.2	981.4	189.5	458.0	65.0	381.3	54.6	51.0
	1975-1	13046.0	611.5	1605.3	141.6	438.1	79.6	20.4	54.9	8.0	48.7	9.7	29.2	5.3	31.9	5.3	3.1
	1975-3	188160.7	119.6	232.0	27.4	83.7	19.9	6.7	18.9	3.4	16.8	4.1	12.7	2.1	12.7	3.1	0.6
C75-14	1990-1	93586.2	2097.9	4402.5	468.9	1631.9	300.5	79.9	210.5	31.2	189.2	36.3	87.4	13.4	75.6	11.8	9.6
	1990-3	135125.2	3996.9	7705.9	867.0	3082.6	561.1	151.9	395.3	58.4	352.2	67.1	168.7	24.6	145.2	21.7	17.6
	1975-1	133338.5	1370.3	2740.0	295.5	1059.9	188.2	47.6	123.8	18.9	117.0	22.7	53.5	8.2	51.6	8.1	6.1
C75-14	1975-1(2)	161002.8	3574.0	7353.8	775.6	2773.8	494.8	129.1	322.3	48.7	305.5	57.0	137.3	21.1	126.8	18.4	16.1
	1975-3	138686.8	589.5	1123.8	127.3	451.3	84.5	22.1	64.4	10.4	60.7	12.7	31.4	5.0	31.7	5.4	2.6
	1990-1	140322.6	3121.8	6167.8	669.3	2343.1	416.9	108.8	284.0	42.6	267.5	50.7	123.6	18.6	110.5	16.8	13.7
C75-27	1990-3	160050.9	5093.9	9976.8	1077.9	3902.5	677.2	183.9	467.6	69.0	426.5	81.4	199.5	29.3	177.5	25.9	22.4
	1977-1	71481.7	2539.8	5993.6	559.1	1921.8	360.2	95.9	270.5	40.2	253.7	51.3	132.5	20.2	125.0	19.7	12.4
	1977-1(2)	125852.7	2512.3	11763.5	581.4	2258.6	461.3	131.9	325.5	59.3	443.6	105.4	304.9	49.0	326.0	50.5	19.4
C75-11	1977-2	38701.9	411.3	1192.1	90.3	316.3	62.5	16.7	45.6	6.6	47.2	10.3	28.9	4.8	33.9	5.6	2.3
	1990-2	116444.7	179.7	345.6	36.7	118.1	23.7	4.7	21.0	2.6	19.2	3.8	11.2	1.8	11.1	2.3	0.8
	1975-1	105500.0	1666.6	3447.6	360.6	1248.8	234.0	63.0	169.7	24.9	141.7	29.0	73.5	10.6	65.1	9.3	7.5
C75-11	1975-2	177759.3	1686.2	3210.3	341.3	1259.6	230.6	63.8	180.9	26.6	162.0	32.0	80.5	11.5	68.7	11.2	7.4
	1975-3	55127.2	372.6	711.1	75.0	259.5	51.7	13.9	41.0	5.2	30.8	6.3	14.9	2.2	12.5	2.5	1.6
	1996-1	60997.9	1310.6	2623.1	269.5	916.1	168.1	46.3	120.6	17.9	106.4	20.1	48.3	7.3	41.6	6.8	5.7
C75-14	1996-2	59619.9	924.9	1847.2	190.9	699.2	129.9	35.5	93.8	13.2	78.4	15.6	38.8	5.7	33.2	5.4	4.1
	1996-3	158381.3	5235.5	9378.6	986.4	3493.6	653.1	177.0	485.5	68.5	398.4	76.7	184.1	26.5	155.7	23.6	21.3
	Soil	669344.0	29785.8	58902.3	6693.4	25100.4	4350.7	1338.7	4016.1	669.3	2677.4	669.3	1338.7	–	1004.0	–	136.5
C76-1	Soil	859106.5	32646.0	64528.4	7254.7	27681.3	4772.8	1336.4	4200.1	572.7	3054.6	572.7	1527.3	190.9	1145.5	190.9	149.7
C75-12	1985 crust	105063.6	6944.4	14273.3	1511.9	5714.4	1050.6	256.3	948.1	128.1	691.9	128.1	384.4	51.3	333.1	51.3	32.5

Sample code as in Table 1.

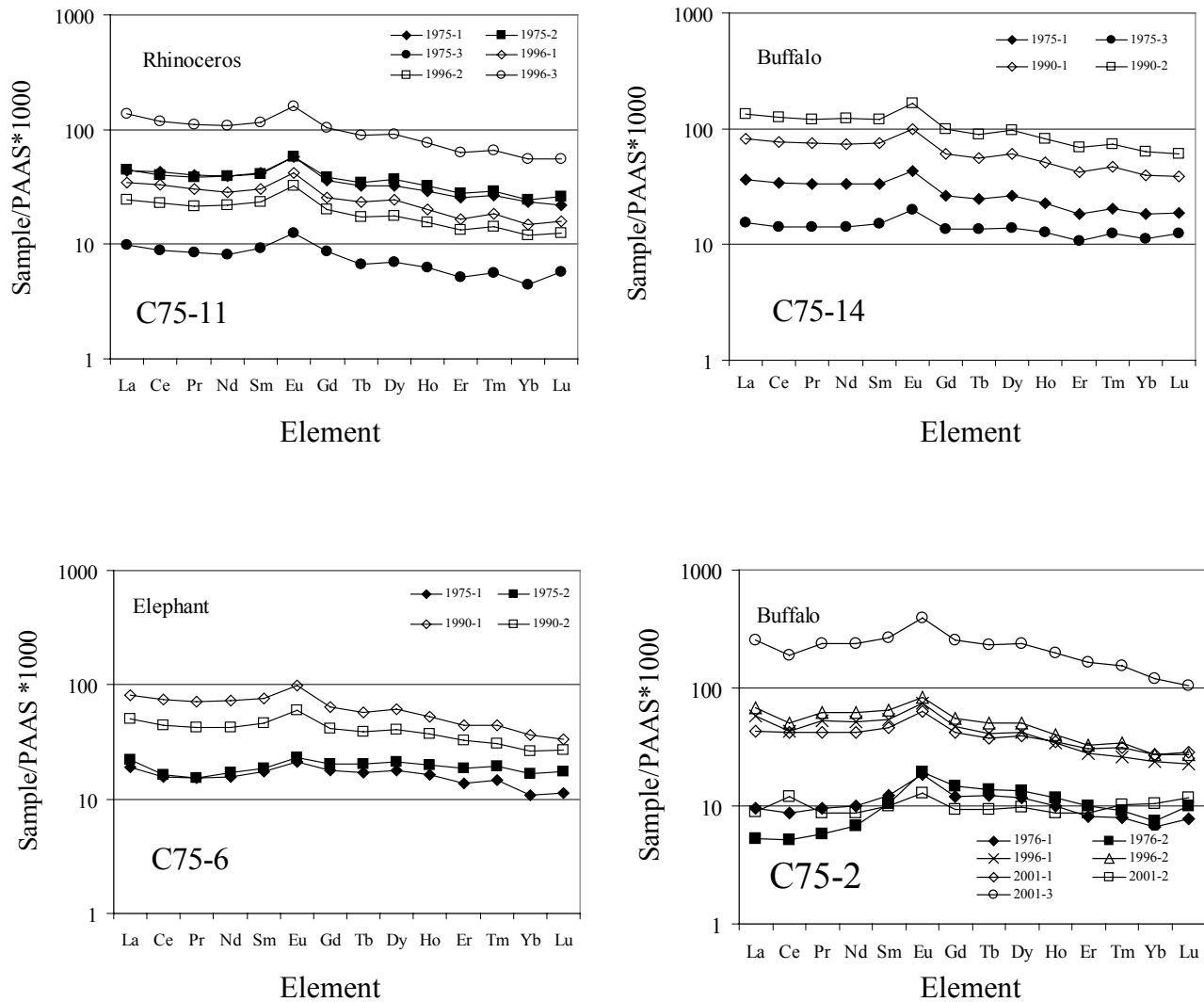


Fig. 5. Shale (PAAS) normalized REE contents in bones from Amboseli. Sizes (length and width) of crystals disaggregated from bone surfaces in skeletons C75-11 (A), C75-12 (B), C75-27 (C) and C75-6 (D). Samples taken from the initial (filled symbols) and final (open symbols) years of collection, and from surface bone (diamonds), sub-surface cortical bone (squares) and trabecular bone (circles).

on the soil surface. In some bones the organic content is reduced by 50% in 15 years. As type 1 collagen is the major component of the organic material in bone, this reduction in organic content presumably involves significant hydrolysis of collagen. There is also clear evidence from both direct observation of disaggregated bone mineral crystals through TEM, and indirect evidence from the changes in the IR splitting factor of bone mineral, that the dahllite crystals associated with the bone surface increase in size after extended exposure. There is a strong correlation between crystallinity (IRSF) and mean crystal size (Fig. 4), and a clear relationship between crystallinity and organic content (Fig. 8). This is direct evidence that crystallinity (as measured by the IRSF) is primarily controlled by mean crystal size, and that post-mortem alterations in bone crystal size are closely related to decomposition of the collagen matrix. A similar conclusion was reached by

Roberts et al. [36], who showed a very strong correlation between protein content and crystallinity in experimentally boiled bone, and a weaker relationship in archaeological bones from various sites. There is good theoretical and empirical evidence to suggest that once removed from the organic matrix, bone crystallites experience simultaneous dissolution and growth in a manner analogous to Ostwald ripening [28,31,48], where large crystals grow at the expense of smaller crystallites. This is clearly supported by the strong relationship between IRSF and organic content seen in bones from Amboseli and elsewhere, and represents a fundamental property of bone. Once removed from biological control, bone crystallites will spontaneously grow by Ostwald ripening, unless this process is inhibited by the organic matrix. Thus, as the organic matrix is broken down, bone crystallites increase in size. Increases in mean crystal length are therefore a result of

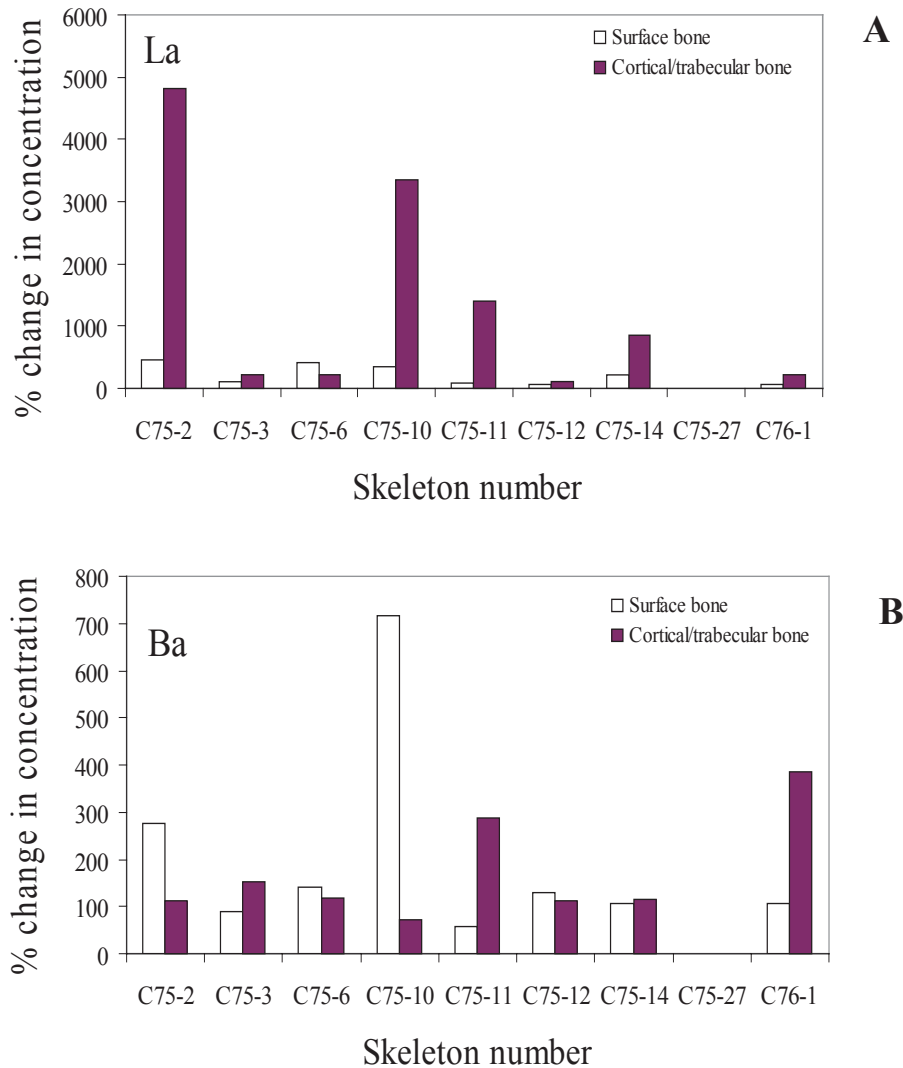


Fig. 6. Increase in La (A) and Ba (B) concentrations in bone through the sample period expressed as percent change from initial conditions. Samples taken from surface bone (open blocks) and sub-surface cortical bone (filled blocks). Note larger change in La concentrations compared to Ba, and greater La uptake in sub-surface cortical bone compared to surface bone.

both loss of smaller crystals and growth of larger crystals.

Recently, Reiche et al. [35] observed complex changes in apatite crystal size and shape in a sample of bones from different depositional localities and found no significant relationship between IRSF and mean crystal length. Similarly, Hedges et al. [17] did not find any correlation between crystallinity and protein content in a suite of 40 archaeological bones from three localities. They argued that loss of protein in these bones was independent of both microbial attack and chemical change, and that the timescales of each process must be significantly different. Both of these studies, however, were based on bones recovered from a range of depositional localities with different physico-chemical and microbiological conditions. It is likely that such varying depositional conditions influence the relative rates and mechanisms of organic decomposition and mineral re-

crystallization and thus obscure the relationship between organic decomposition and crystal size increase documented in the Amboseli bones (e.g. [29]).

4.2. Hydrology of bone alteration

The distribution of authigenic minerals developed within bones from Amboseli indicates passage of water through the bone. Trona is a very soluble mineral that forms under evaporitic conditions. Its presence as a crust on the exposed surfaces of some bones strongly suggests that these are sites of evaporation of water containing dissolved carbonate and sodium. Bones resting on soil surfaces are in partial contact with alkaline pore waters, and as water is lost from the upper exposed surface of the bone, soil pore-waters will be drawn upward through the bone.

Barite is found in more than half of all of the examined bones and is extensively developed within

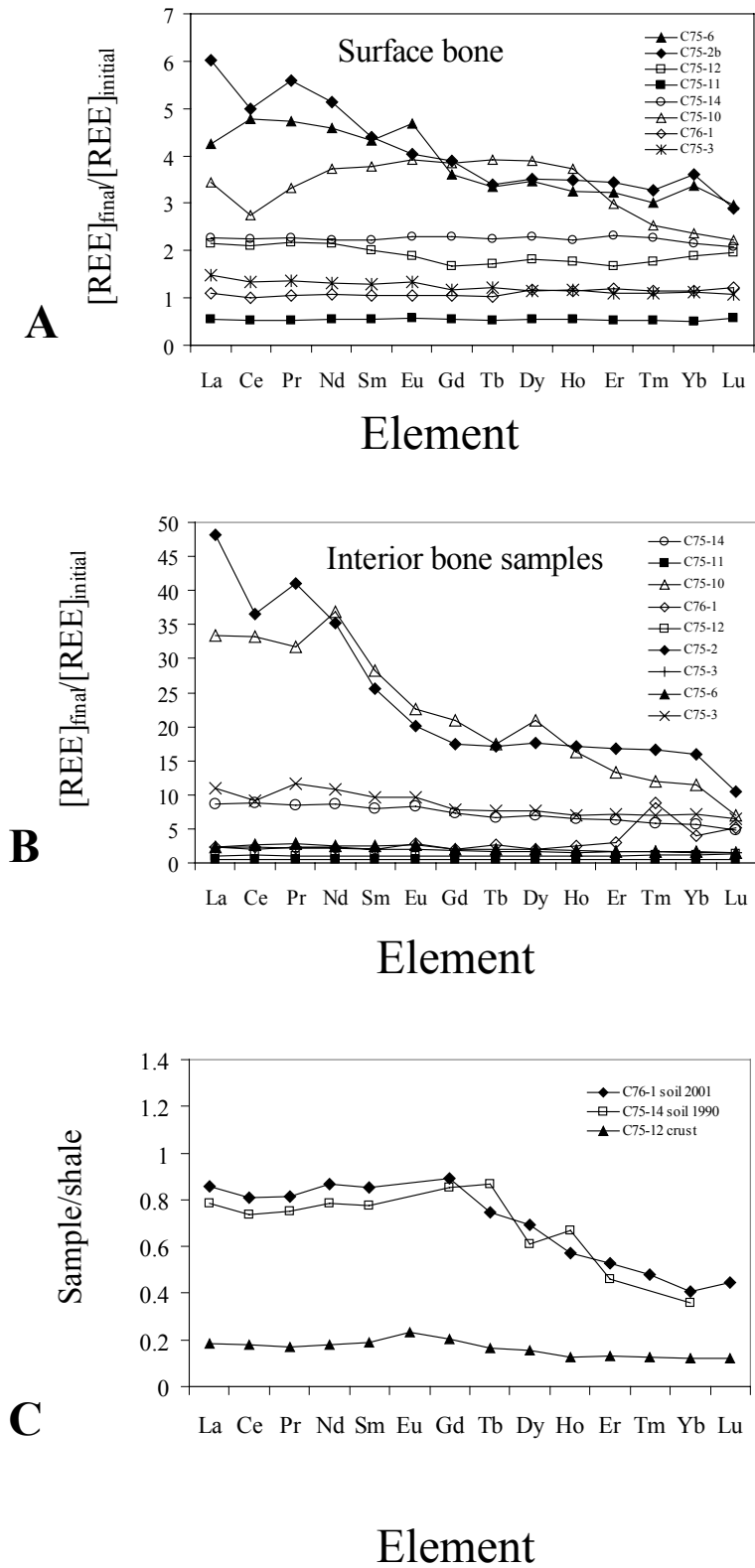


Fig. 7. Uptake of REE into bone (given by final/initial REE concentration). A: Surface bone samples, B: sub-surface cortical bone samples. Note two patterns of uptake in both cases, one essentially flat with low total increases in REE content, and a second pattern with higher total increases and preferential increase in light REE. Variation in uptake patterns among sampled carcasses may represent a combination of pore water composition, hydrology, and weathering state at the beginning of the observation period. C: Shale (PAAS)-normalized REE patterns of sediment and mineral crust associated with bones C76-1 (2001), C75-14 (1990) and C75-12 (1985).

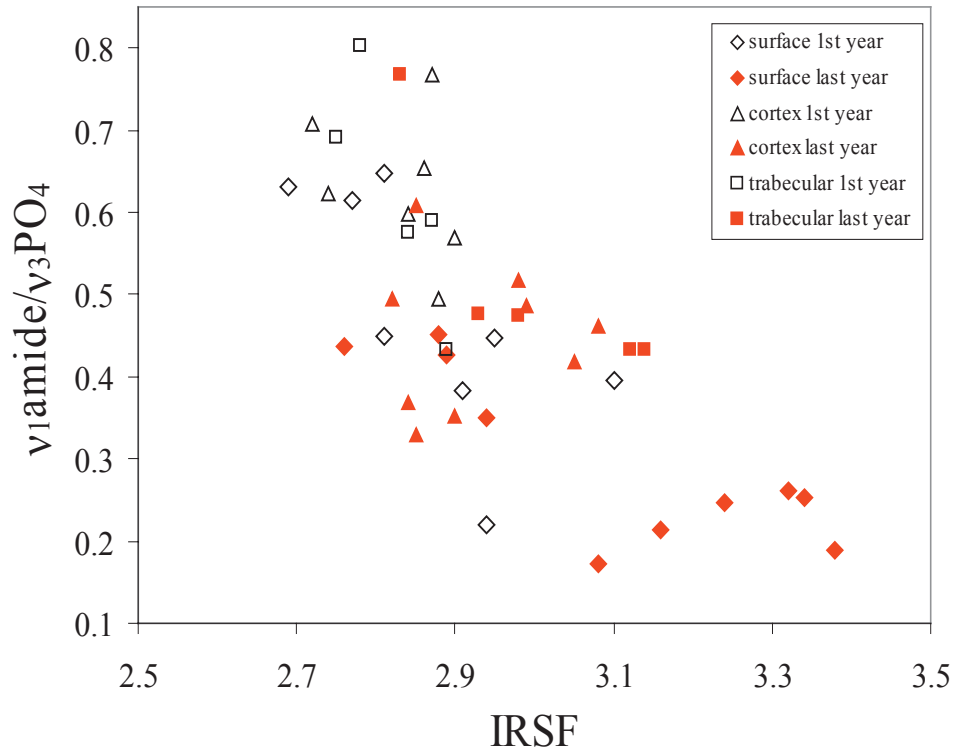


Fig. 8. Relationship between IRSF and $v_1\text{Amide}/v_3\text{PO}_4$ absorbance ratios. Samples collected from the initial (open symbols) and final (filled symbols) years of collection, from surface bone (diamonds) sub-surface cortical bone (triangles) and trabecular bone (squares). Note increase in IRSF and decrease in $v_1\text{Amide}/v_3\text{PO}_4$ ratios with increasing exposure, and that the maximum changes are associated with surface bone samples.

2 years post-mortem in some cases (e.g. skeleton C75-6). The initial concentration of Ba in the bone mineral is less than 50 ppm, so the source of diagenetic Ba cannot be the bone itself, as this would imply widespread dissolution of bone mineral. Additional diagenetic barium must therefore be derived from the soil water. The concentration of Ba in the soil water is relatively low (exchangeable Ba in soil samples <10 ppb), and we therefore conclude that large volumes of water must pass through the bone to account for the widespread occurrence of barite in the void spaces. Biogenic Ba/Ca ratios in bone mineral have been severely altered in under 2 years of exposure on the soil surface.

Authigenic phosphate minerals are rare in the bones from Amboseli, and are found only in bones C75-12 (1990) and within microbial destruction features in bones from C75-11. As there is very little phosphate in the Amboseli sediments (approximately 0.03 wt%, [42]), and possibly less in the pore water, the most likely source of phosphate is dissolution of bone mineral. We believe, however, that the phosphate liberated during this dissolution is immediately involved in growth of adjacent bone crystallites. Therefore, the source of additional phosphate needed to precipitate authigenic crandallite in the pore-spaces of C75-12 remains unknown. Microbial destruction of bone leads to widespread dissolution and redistribution of phosphate

within the bone, and we regard this as the most probable explanation for the authigenic dahllite seen in C75-11.

4.3. Trace element concentrations

The concentration of the REE in bones exposed in Amboseli Park increased by up to one order of magnitude during 15–30 years of exposure. The relative concentrations of REE added to bone do not mirror their concentrations in sediment (Fig. 7), suggesting that the REE were derived from pore waters. Adsorption coefficients for the REE between water and apatite surfaces are very high (10^6 [22]). REE are therefore readily removed from pore waters via adsorption on to bone crystallite surfaces during passage of pore waters through bone [10,34]. The total REE added to cortical and surface portions of bones from Amboseli averages around 5 ppm in most cases (Table 2). Assuming that REE concentrations in pore waters average 1 ppb (e.g. [14,20,50]), and taking density of fresh bone as 2 g/ml, with a porosity of c. $0.1 \text{ cm}^3 \text{ g}^{-1}$ [30], it is possible to calculate the total volume of pore water required to supply the REE to the bone. This simple calculation suggests that to achieve the required increase in REE concentrations over 15 years, bone pore waters must be completely recharged on average once per day. The highest observed increases in REE concentrations in

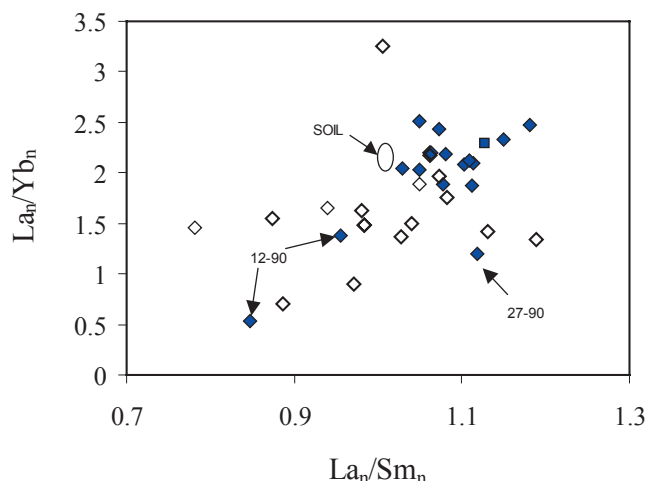


Fig. 9. Weathering-induced changes in REE content in bones from Amboseli. Note that bones sampled in the first year of collection (open diamonds) show relatively consistent La/Yb values, but varied La/Sm values. Bones from the last year of collection show relatively consistent REE patterns. REE patterns of soils from sites C76-1 and C75-14 are indicated by the open ellipse. Subscript 'n' refers to shale (PAAS) normalized values.

trabecular bone would require even greater water flux. This suggests an additional source of REE, most likely derived from REE adsorbed on to sediment particles held within pore spaces of the bone.

In four out of five sample series with sufficient analyses, the lowest total increases in adsorbed REE concentrations were found in the surface sample of bone rather than the deeper cortical portions of the bone. This suggests that waters reaching the evaporative surface of the bones are depleted in REE compared to soil waters due to the efficient removal of REE by adsorption on to bone crystallites. The upper (exposed) surface of weathered bone may therefore show lower total REE concentrations than the lower or internal surfaces. It is interesting to note that concentrations of barium in bone mineral are relatively evenly distributed throughout the bones. This probably reflects the fact that Ba is less readily adsorbed on to bone crystals than the REE, and that the distribution of Ba within bones is partly controlled by precipitation of barite following release of sulphate from decomposing organic materials.

The relative concentrations of REE in fresh bones from Amboseli are varied. Shale normalized La/Yb ratios are fairly consistent for all bones in the initial year of sampling, but La/Sm ratios show wide variation (Fig. 9). The reasons for this variation are unknown, but most likely biogenic. After prolonged exposure, however, all bones trend toward similar REE distribution patterns, enriched in LREE with respect to initial compositions. Significantly, bones trend towards REE compositions that are enriched in middle REE (e.g. Sm) with respect to the sediment (Fig. 9). These observations support the suggestion that REE added to bone were

derived from soil pore waters rather than directly from sediment and/or dust. With increased exposure and exchange with pore waters, therefore, bones inherit a common trace element composition, reflecting the trace element composition and chemistry of the pore water. This observation confirms the use of trace element composition of ancient bone as a natural tag indicating the original location and environment of burial (e.g. [32,44,46]).

5. A model for diagenesis of bones exposed on soil surfaces

Most of the observed diagenetic changes are associated with the bone surface (e.g. Fig. 8). The presence of the highly soluble mineral trona on the surface implies that this is a site of evaporation, and the infiltration of the bone with barite demonstrates that the source of water is mainly from the ground. The changes in bone mineral crystallinity and crystallite dimensions show that the bone itself is subject to chemical diagenesis. We thus propose a model for diagenesis involving the dynamic interaction of bones, soil moisture, and evaporation at the ground surface. A bone resting on the soil surface draws up pore water, this pore water evaporates at the exposed upper surfaces of the bone, and the bone is thus subjected to a dynamic hydrological regime. This process can be compared to the 'wicking' mechanism in an oil lamp or candle. Evaporation of water at the bone/air interface is the driving force for active flow of water through the bone, and the high surface area of pore spaces in the bone makes it an effective wick. Major changes in bone mineral and the organic matrix appear to be caused by this hydrological 'wicking' mechanism within a relatively short time span (i.e., in some cases as little as 2 years).

We tested the feasibility of this model by immersing the end of an elongated piece of slightly weathered (weathering stage 1, [2]) sub-recent bovine cortical bone in an aqueous solution containing a dye. Water was taken up into the bone rapidly, within 20 h capillary action had drawn the water up to a height of 3.1 centimeters above the water surface, after which point no further uptake occurred. The volume of water taken up by the bone was to approximately $0.08 \text{ cm}^3 \text{ g}^{-1}$. The total volume porosity of modern bone is approximately $0.13 \text{ cm}^3 \text{ g}^{-1}$ [30], and thus it is likely that the internal pore space within the bone approached saturation within 20 h, after which no further uptake of water occurred. This experiment was performed in a humid environment, where evaporation of water from the bone surface was minimized. In arid environments, water will be lost from bone surfaces, and further water will be continuously drawn up, maintaining near saturation conditions within the bone. It is possible that bones become increasingly effective wicks in the early years

post-mortem, as organic matter begins to decay and opens up more connected pore spaces, whereas wicking efficiency declines later in the weathering sequence when the bone starts to fall apart.

The essentially hydrological driving mechanism of diagenesis for exposed bone proposed above cannot fully account for the observed dissolution of bone mineral. Bone mineral is highly insoluble above pH 8, and the presence of calcite in many examined bones shows that the pH within void spaces must have been above 8. It is therefore unlikely that pore waters moving through the bone would promote sufficient dissolution of dahllite to account for the observed increases in maximum and mean bone crystal sizes.

The exposed surfaces of bones show the largest changes in protein content and crystallinity, suggesting that degradation of collagen (and consequent alterations in bone mineral) is driven by temperature fluctuations and the effect of UV light on the collagen framework, coupled with the dynamic hydrological environment described above. We propose that hydrolysis of the collagen matrix provides an additional driving mechanism for dissolution of bone crystallites. Hydrolysis of collagen, and the presence of rainwater, potentially supplies protons that may facilitate bone mineral dissolution. This probably occurs at or close to the site of hydrolysis and not in the voids where the pH is buffered by the carbonate–bicarbonate system. Phosphate released during crystal dissolution may then be involved in recrystallization of the remaining bone dahllite crystals, whose reactive surfaces are exposed following collagen hydrolysis.

6. Broader implications

Recrystallization of bone dahllite involves addition of calcium phosphate to the remaining crystals, essentially a process of crystal cannibalization. This means that any trace metal ions present in pore waters within the bone may be incorporated into the newly formed crystal lattice, and that ions previously adsorbed on to crystal surfaces may be incorporated into the new crystal lattice during growth. In either case, added cations will be associated with the dahllite crystal lattice and therefore cannot be removed through sequential acid washing techniques [40]. This point was made by Tuross et al. [47], and is strengthened by the present study. Furthermore, where available, recrystallization of bone may incorporate phosphate and/or carbonate ions from groundwater. In this case, the stable isotope ($\delta^{18}\text{O}$, $\delta^{13}\text{C}$) ratios of bone will be altered during diagenesis. In an earlier study of the same bone samples from Amboseli, Koch et al. [24] found no systematic change in the stable isotope composition of bone mineral over time. Relatively deep (>5 mm) holes were drilled into the bone to collect bone powder by Koch et al. [24], however, and

thus this study sampled less altered portions of the bone. Furthermore, pore waters at Amboseli have very low concentrations of dissolved phosphate, and soil phosphate is unlikely to contribute significantly to growth of bone crystallites.

Obviously, chemical diagenesis continues once the bones are buried. The driving forces for alteration of buried bones may differ from sub-aerially exposed bones, particularly where the hydrological regime changes. In particular, the volume of water flowing through a bone is likely to be less in a burial environment than in a bone lying on a soil surface. From our observations in various prehistoric caves, a major driving force of early chemical diagenesis in general is decomposition of organic material that introduces acid into the sediments, including the buried bones [21]. In addition to this external source of acid, the bone matrix continues to degrade and acts as an internal source of acid. Therefore, the amount of organic material left in the bone once it is buried will have an effect on the diagenetic environment; the longer the bone weathers on the surface, the lower the potential post-burial acidity, and the greater the dependency on external sources of phosphate to fill in the 20–30% pore space originally occupied by the organic matrix.

All investigations in this study were conducted on bone *sensu stricto*. Bone, dentin and enamel behave differently in any depositional environment, as the factors controlling the degree and rate of chemical alteration in phosphate biominerals are crystal size, organic content and hydrology or water flow. Bone and dentin are similar in terms of crystal size, composition and organic content, and thus are equally vulnerable to crystal dissolution and alteration; however, capping enamel may restrict the flow of water through dentin. Enamel, by virtue of its large crystal size and low organic content, is relatively resistant to post-mortem alteration. It should be noted, however, that enamel is not immune from diagenetic alteration: fossil enamel typically contains 1–3 orders of magnitude higher concentrations of trace elements such as the REE in the crystal lattice [46].

7. Summary

- Bones exposed on the soil surface in a tropical grassland environment suffered extensive mineralogical and chemical alteration within 15 years or less post-mortem.
- The destruction of the organic matrix of bone (collagen) appears to facilitate dissolution of dahllite crystallites. The phosphate liberated by this dissolution is involved in growth of exposed bone crystallites, leading to an increase in mean and maximum crystallite size.

- In the tropical environment of Amboseli, water flow is driven by evaporative transport through the bone in a process analogous to the wicking of a candle. Cations introduced into the bone/water system during passage of pore waters may be either adsorbed on to exposed bone crystallites, or incorporated into authigenic minerals.
- The trace element composition of bone mineral may be extensively and irrevocably altered within a few years post-mortem, trending towards a composition that reflects the chemistry of the local pore waters.
- Permineralization (growth of authigenic minerals in pore spaces in bones after death) occurred extensively within as little as two years post-mortem in our study, and is certainly not diagnostic of post-burial alteration of the bone mineral itself. Decomposition of the organic matrix, growth of bone crystallites, and growth of authigenic minerals are all particularly rapid at exposed, evaporative surfaces of bones.
- Understanding the processes of diagenesis will help in the difficult task of extracting original (biogenic) geochemical signals from ancient bone, and also helps to refine the use of post-mortem chemical change in bone as a proxy for environmental conditions.

Acknowledgements

We would like to thank Talmon Arad of the Weizmann Institute of Science for his patient and skilled help in all aspects of TEM microscopy and Don Dean of the Department of Paleobiology, Smithsonian Institution for his technical skill in making the thin sections. C.T. was supported by the Smithsonian Institution postdoctoral fellowship program. The Amboseli bone project has been supported by the National Geographic Society (Grants # 1508 and #4339-90). Dr David Western, the Kenya Wildlife Service and the National Museums of Kenya have provided valuable advice and assistance throughout the course of this project. This study was also supported by a grant (No. 302/00) from the Israel Science Foundation to S.W., as well as by a Burch Fellowship to S.W. from the Smithsonian Institution. S.W. is the incumbent of the Dr Walter and Dr Trude Borchardt Professorial Chair in Structural Biology.

Appendix A. Analytical techniques

A.1. Fourier transform infrared spectroscopy (FTIR)

Spectra were obtained following the method of Weiner and Bar-Yosef [52] before and after treatment with sodium acetate/acetic acid buffer solution (pH 5)

and used to derive the splitting factor (IRSF) [52] (Fig. 1A). Errors (estimated by $5\times$ preparation and analysis of single samples) are ± 0.05 in fresh bone increasing to ± 0.2 in weathered bone. The carbonate content of each bone sample was estimated using the method of Wright and Schwartz [55]. The ratio of the Amide-1 and $\nu_3\text{PO}_4$ absorptions at wavelengths 1640 and 1035 cm^{-1} respectively was used as an estimate of bone protein concentration (e.g. [41]). The error associated with this measurement is estimated as ± 0.06 in fresh bone, and ± 0.09 in weathered bone. FTIR spectra were also used for mineral identification.

A.2. Thermogravimetric analysis (TGA) and differential thermal analysis (DTA)

Approximately 0.05 g of acid treated bone powder was placed in a platinum crucible and heated to $1000\text{ }^\circ\text{C}$ at a rate of $20\text{ }^\circ\text{C}$ per minute. The heating was performed in a Shimadzu DTG-50 instrument equipped with a microbalance. Weight was monitored throughout the analyses. Collagen decomposes thermally between $250\text{--}500\text{ }^\circ\text{C}$, and weight of organic materials in a bone was defined as the percent change in weight between 200 and $550\text{ }^\circ\text{C}$ (Fig. 2). TGA analysis of bone standard NIST 1486 gave 27% organic content consistent with the certified value.

A.3. Transmission electron microscopy (TEM) of bone crystals

The method used is based on method 2 of Weiner and Price [51]. Samples were examined in a Philips Technai-12 electron microscope operated at 100 keV, and digital images were taken at $96,000\times$ magnification. For each crystal the longest dimension (length) and the dimension perpendicular to this (width) were measured using NIH-Image software. The crystals selected for measurement were either separated crystals, in which the entire periphery was visible, or partially overlapped crystals, where at least three of four edges were visible and maximum dimensions could be determined. In all cases at least 50 single crystals (according to criterion 2 of Ziv and Weiner [56]) were measured, and in most cases 100 crystals were measured.

A.4. Inductively coupled plasma–mass spectrometry (ICP–MS) analyses

Rare earth element (REE) and barium contents of bone samples were determined by ICP–MS. Samples of bone powder were lyophilized, and 0.05–0.1 g of powder was accurately weighed into polypropylene vessels. Approximately 3 ml of sodium acetate buffer (pH 5) was added, and left overnight. The buffer was decanted after

centrifugation, and the resulting pellet of bone mineral was freeze-dried and reweighed. The cleaned bone mineral pellet was dissolved in about 3 ml of 3 N HCl. The resulting solution was centrifuged, the supernatant removed, and filtered through a 0.2 µm filter. The filtered liquid was then made up to 50 ml with 1% HNO₃, and an internal standard of Re and Ru added to give a final concentration of 1 ppb.

The solution (500–1000 × dilution of original bone) was analyzed using a Perkin Elmer ELAN 6000 ICP–MS operating in peak hopping mode. Reported concentrations are the mean of three analyses, and analyses were rejected if relative standard deviations exceeded 5%. NIST 120C (Florida Phosphate) and 1486 (bovine bone) were prepared as above, and used as standards to monitor accuracy and precision. Measured values in all cases are within 10% of expected values. Exchangeable trace elements in soils were measured by reacting c. 0.5 g crushed weighed soil powder with c. 3 ml 1 N HCl. Resulting suspension was centrifuged, the supernatant decanted and made up to 50ml with 1% HNO₃, and analyzed by ICP–MS. REE concentrations were normalized to post Archaean average shale (PAAS) values [43].

References

- [1] R.E. Barrick, W.J. Showers, A.G. Fischer, Comparison of thermoregulation of four ornithischian dinosaurs and a varanid lizard from the Cretaceous Two Medicine Formation: evidence from oxygen isotopes, *Palaio* 11 (1996) 295–305.
- [2] A.K. Behrensmeyer, Taphonomic and ecological information from bone weathering, *Paleobiology* 4 (1978) 150–162.
- [3] A.K. Behrensmeyer, Terrestrial vertebrate accumulations, in: P. Allison, D.E.G. Briggs (Eds.), *Taphonomy: Releasing the Data Locked in the Fossil Record*, Plenum, New York, 1991, pp. 291–335.
- [4] A.K. Behrensmeyer, The bones of Amboseli, *National Geographic Research and Exploration* 9 (1993) 402–421.
- [5] A.K. Behrensmeyer, D. Western, D.E. Dechant Boaz, New perspectives in paleoecology from a recent bone assemblage, Amboseli Park, Kenya, *Paleobiology* 5 (1979) 12–21.
- [6] A.K. Behrensmeyer, D.E. Dechant Boaz, The recent bones of Amboseli National Park, Kenya, in: A.K. Behrensmeyer, A. Hill (Eds.), *Fossils in The Making*, University of Chicago Press, Chicago, 1980, pp. 72–92.
- [7] A.K. Behrensmeyer, A. Hill, *Fossils in The Making*, University of Chicago Press, Chicago, 1980.
- [8] L.S. Bell, M.F. Skinner, S.J. Jones, The speed of post mortem change to the human skeleton and its taphonomic significance, *Forensic Science International* 82 (1996) 129–140.
- [9] J.D. Bryant, B. Luz, P.N. Froelich, Oxygen isotope composition of fossil horse tooth phosphate as a record of continental paleoclimate, *Palaeogeography, Palaeoclimatology, Palaeoecology* 107 (1994) 303–316.
- [10] X-B. Chen, J.V. Wright, J.L. Conca, L.M. Peurrung, Effects of pH on heavy metal sorption on mineral apatite, *Environmental Science and Technology* 31 (1997) 624–631.
- [11] A.M. Child, Microbial taphonomy of archaeological bone, *Studies in Conservation* 40 (1995) 19–30.
- [12] M.J. Collins, A.M. Gernaey, C.M. Nielsen-Marsh, C. Vermeer, P. Westbroek, Slow rates of degradation of osteocalcin: Green light for fossil bone protein? *Geology* 28 (2000) 1139–1142.
- [13] M.J. Collins, C.M. Nielsen-Marsh, J. Hiller, C.I. Smith, J.P. Roberts, R.V. Prigodich, T.J. Weiss, J. Csapo, A.R. Millard, G. Turner-Walker, The survival of organic matter in bone: A review, *Archaeometry* 44 (2002) 383–394.
- [14] B. Dupré, J. Gaillardet, D. Rousseau, C.J. Allègre, Major and trace elements of river-bourne material: The Congo Basin, *Geochimica et Cosmochimica Acta* 60 (1996) 1301–1321.
- [15] G. Grupe, T.D. Price, P. Schroter, F. Sollner, Mobility of Bell Beaker people revealed by Sr isotope ratios of tooth and bone: a study of southern Bavarian skeletal materials, *Applied Geochemistry* 12 (1999) 517–525.
- [16] R.L. Hay, R.E. Hughes, T.K. Kyser, H.D. Glass, J. Liu, Magnesium-rich clays of the Meerschaum mines in the Amboseli Basin, Tanzania and Kenya, *Clays and Clay Minerals* 43 (1995) 455–466.
- [17] R.E.M. Hedges, A.R. Millard, A.W.G. Pike, Measurements and relationships of diagenetic alteration of bone from three archaeological sites, *Journal of Archaeological Science* 22 (1995) 201–209.
- [18] C.J. Hackett, Microscopical focal destruction (tunnels) in excavated human bones, *Medicine, Science and the Law* 21 (1981) 243–265.
- [19] K.A. Hoppe, P.L. Koch, R.W. Carlson, S.D. Webb, Tracking mammoths and mastodons: reconstruction of migratory behaviour using strontium isotope ratios, *Geology* 27 (1999) 439–442.
- [20] K.H. Johannesson, M.J. Hendry, Rare earth element geochemistry of groundwaters from a thick till and clay-rich aquitard sequence, Saskatchewan, Canada, *Geochimica et Cosmochimica Acta* 64 (2000) 1493–1509.
- [21] P. Karkanas, O. Bar-Josef, P. Goldberg, S. Weiner, Diagenesis in prehistoric caves: the use of minerals that form in situ to assess the completeness of the archaeological record, *Journal of Archaeological Science* 27 (2000) 915–929.
- [22] D. Koeppenkastrop, E.H. DeCarlo, Sorption of rare-earth elements from seawater onto synthetic mineral particles—an experimental approach, *Chemical Geology* 95 (1992) 251–263.
- [23] P.L. Koch, A.N. Halliday, L.M. Walter, R.F. Stearley, T.J. Huston, G.R. Smith, Sr isotopic composition of hydroxyapatite from Recent and fossil salmon: the record of lifetime migration and diagenesis, *Earth and Planetary Science Letters* 108 (1992) 277–287.
- [24] P.L. Koch, A.K. Behrensmeyer, A.W. Stott, N. Tuross, R.P. Evershed, M.L. Fogel, The effects of weathering on the stable isotope composition of bones, *Ancient Biomolecules* 3 (2001) 117–134.
- [25] Y. Kolodny, B. Luz, M. Sander, W.A. Clemens, Dinosaur bones: fossils or pseudomorphs? The pitfalls of physiology reconstruction from apatitic fossils, *Palaeogeography, Palaeoclimatology, Palaeoecology* 126 (1996) 161–171.
- [26] A. Longinelli, Oxygen isotopes in mammal bone phosphate: a new tool for paleohydrological and paleoclimatological research? *Geochimica et Cosmochimica Acta* 48 (1984) 385–390.
- [27] A.R. Millard, R.E.M. Hedges, A diffusion-adsorption model of uranium uptake by archaeological bone, *Geochimica et Cosmochimica Acta* 60 (1999) 2139–2152.
- [28] J. Moradian-Oldak, Interactions between acidic macromolecules and different calcium phosphate crystals: Relevance to carbonate apatite formation in biomineralization. PhD Thesis, Weizmann Institute of Science, Rehovot, Israel, 1992.
- [29] C.N. Nielsen-Marsh, R.E.M. Hedges, Patterns of diagenesis in bone I: The effects of site environments, *Journal of Archaeological Science* 27 (2000) 1139–1150.

- [30] C.M. Nielsen-Marsh, A.M. Gernaey, G. Turner-Walker, R.E.M. Hedges, A.W.G. Pike, M.J. Collins, The chemical degradation of bone, in: M. Cox, S. Mays (Eds.), *Human Osteology in Archaeology and Forensic Science*, Greenwich Medical Media, London, 2000, pp. 439–454.
- [31] W.Z. Ostwald, *Physical Chemistry* 22 (1879) 289.
- [32] T.W. Plummer, A.M. Kinuyua, R. Potts, Provenancing of hominid and mammalian fossils from Kanjera, Kenya, using EDXRF, *Journal of Archaeological Science* 21 (1994) 553–563.
- [33] T.D. Price, Multi-element studies of diagenesis in prehistoric bone, in: T.D. Price (Ed.), *The Chemistry of Prehistoric Human Bone*, Cambridge University Press, Cambridge, 1989, pp. 126–154.
- [34] B. Reynard, C. Lécuyer, P. Grandjean, Crystal chemical controls on rare-earth element concentrations in fossil biogenic apatites and implications for paleoenvironmental reconstructions, *Chemical Geology* 155 (1999) 233–241.
- [35] I. Reiche, C. Vignaud, M. Menu, The crystallinity of ancient bone and dentine: New insights by transmission electron microscopy, *Archaeometry* 44 (2002) 447–459.
- [36] S.J. Roberts, C.I. Smith, A. Millard, M.J. Collins, The taphonomy of cooked bone: Characterizing boiling and its physico-chemical effects, *Archaeometry* 44 (2002) 485–494.
- [37] S. Safont, A. Malgosa, M.E. Subira, J. Gilbert, Can trace elements in fossils provide information about palaeodiet? *International Journal of Osteoarchaeology* 8 (1998) 23–37.
- [38] M.H. Schweitzer, C. Johnson, T.G. Zocco, J.R. Horner, J.R. Starkey, Preservation of biomolecules in cancellous bone of *Tyrannosaurus rex*, *Journal of Vertebrate Paleontology* 17 (1997) 349–359.
- [39] A. Sillen, Biogenic and diagenetic Sr/Ca in Plio-Pleistocene fossils of the Omo Shungura Formation, *Paleobiology* 12 (1986) 311–323.
- [40] A. Sillen, J.C. Sealey, Diagenesis of Sr in bone: a reconsideration of Nelson et al. (1986), *Journal of Archaeological Science* 22 (1995) 313–320.
- [41] M.C. Stiner, S.L. Kuhn, S. Weiner, O. Bar-Yosef, Differential burning, recrystallization, and fragmentation of archaeological bone, *Journal of Archaeological Science* 22 (1995) 223–237.
- [42] R.K. Stoessell, R.L. Hay, The Geochemical origin of sepiolite and kerolite at Amboseli, Kenya, *Contributions to Mineralogy and Petrology* 65 (1978) 255–267.
- [43] S.R. Taylor, S.M. McLennan, *The Continental Crust: Its Composition and Evolution*, Blackwell Scientific, Oxford, 1985.
- [44] C.N. Trueman, M.J. Benton, A geochemical method to trace the taphonomic history of reworked bones in sedimentary settings, *Geology* 25 (1997) 263–266.
- [45] C.N. Trueman, D.M. Martill, The long term preservation of bone: The role of bioerosion, *Archaeometry* 44 (2002) 371–382.
- [46] C.N. Trueman, N. Tuross, Trace elements in recent and fossil bone, in: M.J. Kohn, J. Rakovan, J.M. Hughes (Eds.), *Phosphates: Geochemical, Geobiological and Materials Importance*. Mineralogical Society of America, *Reviews in Mineralogy and Geochemistry* 48 (2002) 489–521.
- [47] N. Tuross, A.K. Behrensmeyer, E.D. Eanes, Strontium increases and crystallinity changes in taphonomic and archaeological bone, *Journal of Archaeological Science* 16 (1989a) 661–672.
- [48] N. Tuross, A.K. Behrensmeyer, E.D. Eanes, L.W. Fisher, Molecular preservation and crystallographic alterations in a weathering sequence of wildebeest bones, *Applied Geochemistry* 4 (1989b) 261–270.
- [49] G. Turner-Walker, U. Syversen, Quantifying histological changes in archaeological bones using BSE-SEM image analysis, *Archeometry* 44 (2002) 461–468.
- [50] E. Valsami-Jones, K.V. Ragnarsdottir, N.O. Crewe-Read, T. Mann, A.J. Kemp, G.C. Allen, An experimental investigation of the potential of apatite as radioactive and industrial waste scavenger, in: S.H. Bottrell (Ed.), *Fourth International Symposium on the Geochemistry of the Earth's Surface: Yorkshire, United Kingdom*, University of Leeds, Leeds, 1996, pp. 686–689.
- [51] S. Weiner, P.A. Price, Disaggregation of bone into crystals, *Calcified Tissue International* 39 (1986) 365–375.
- [52] S. Weiner, O. Bar-Yosef, States of preservation of bones from prehistoric sites in the Near East: a survey, *Journal of Archaeological Science* 17 (1990) 187–196.
- [53] D. Western, C. Van Praet, Cyclical changes in the habitat and climate of an East African ecosystem, *Nature* 241 (1973) 104–106.
- [54] C.T. Williams, Alteration of chemical composition of fossil bones by soil processes and groundwater, in: G. Grupe, B. Herrmann (Eds.), *Trace Elements in Environmental History*, Springer-Verlag, 1988, pp. 27–40.
- [55] L.E. Wright, H.P. Schwartz, Infrared and isotopic evidence for diagenesis of bone apatite at Dos Pilas, Guatemala: Palaeodietary implications, *Journal of Archaeological Science* 23 (1996) 933–944.
- [56] V. Ziv, S. Weiner, Bone crystal sizes: A comparison of transmission electron microscopic and X-ray diffraction line width broadening techniques, *Connective Tissue Research* 30 (1994) 165–170.